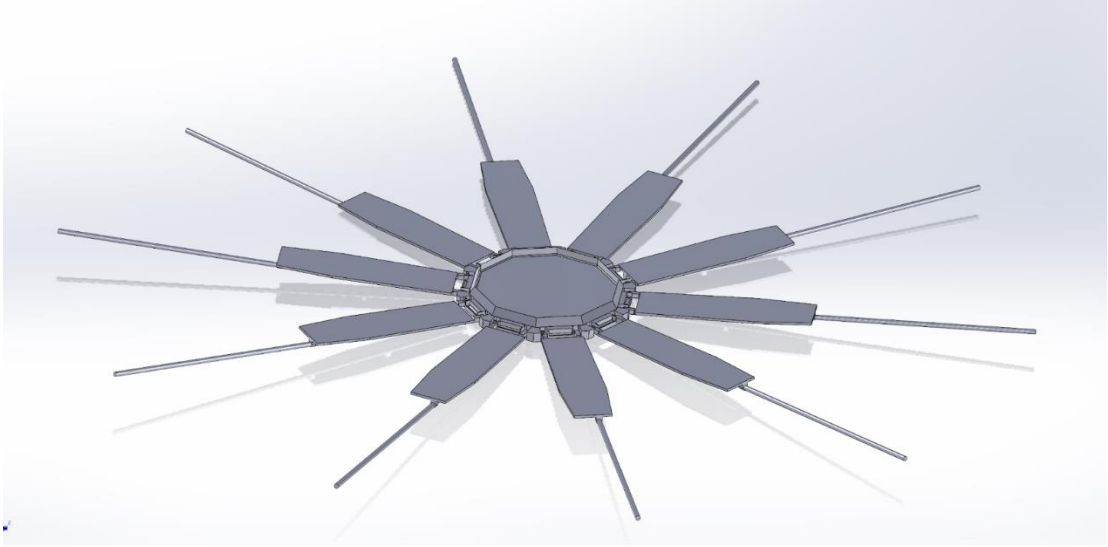

NASA HuLC – TCNJ Adaptable Regolith Retention Platform (TARRP)

Department of Mechanical Engineering, The College of New Jersey

June 05, 2024

Harry Brier[a], John Hardie[b], Christian Katsikis[c], Matt Walsh[d], Aidan Wiehe[e]

[abcde]Undergraduate Student of Mechanical Engineering

Mohammed Alabsi, PhD. – Faculty Advisor

Abstract

The TCNJ Human Lander Challenge team has developed a proof of concept for the implementation of a single use landing platform, constructed from a carbon matrix carbon composite material with a graphite foil. This platform is intended to mitigate the production of ejecta during the powered descent, landing, and ascent of the Human Landing System and Commercial Lunar Payload Services vehicles. By extension, this platform would also reduce the occurrence of ejecta damage to the vehicles themselves and allow for the delivery of mission-critical infrastructure to the lunar surface in service of the upcoming Artemis 3 mission.

As of this writing, final testing was not completed due to several complications which developed with the test environment over the course of initial testing. These issues have since been resolved, however, and TCNJ plans to continue this research through the next academic year. Preliminary testing showed promising results with zero deformation at the center of the platform and an average of 10.8 mm deformation at the immediate edges of the platform. Recommendations for future testing include increasing the size of the test chamber, further refining data collection process through the implementation of additional depth cameras, and material validation to ensure that chosen materials can withstand the extreme temperatures and shear forces of powered descent and ascent.

Table of Contents

Introduction

Plume Surface Interaction is the phenomena that occurs when a rocket plume impinges upon the regolith, or the loose rocky material resting atop bedrock of a surface. This is a pressing concern for the exploration of our solar system as the resulting ejecta from this interaction poses a significant hazard to the vehicle generating the impingement, and any existing infrastructure on the surface. In the lunar case, as the ejecta has the potential to reach escape velocity, orbiting vehicles could also be potentially affected. The purpose of the NASA Human Lander Challenge is to address the problems associated with plume-surface interactions (PSI) in advance of the Artemis missions. The competition includes multiple categories through which to contribute to the understanding of PSI, its tracking and measurement, and ultimately its mitigation.

The TCNJ Human Lander Challenge team has chosen to address this problem via the development of a proof-of-concept for a single-use, deployable landing pad. Tentatively named the TCNJ Adaptable Regolith Retention Platform (TARRP), this solution would serve as a barrier between the regolith surface and the descent vehicle's rocket plume, preventing the rapid erosion of the surface and mitigating the risks to the lander. During the planned buildup of assets on the lunar surface over the course of the Artemis missions via the CLPS initiative and, given the enormous cost and complexity of delivering these assets to their operating environment, it is essential to maximize their mean time to failure. The Apollo missions demonstrated that the mean time to failure is significantly reduced by the presence of lunar dust within operational components of hardware on the moon. Promising research is currently in progress to more permanently address the problems associated with PSI, such as rapid regolith sintering to construct landing pads and building materials in situ, however these solutions require an infrastructural footprint on the lunar surface. In order to effectively deliver this infrastructure without incurring damage or reducing their effective service life, a stopgap measure is required. This is the proposed use case for the TARRP.

TARRP Design

The TARRP (Figure 1) consists of a decagonal base plate and polygonal fin assembly with hollow aluminum rods extending radially outward from the fins. These rods support a flexible foil / felt atop the baseplate and fin assembly, intended to cover the interstitial area between the fins. The initial design includes a deployment mechanism consisting of torsional springs stored in compression and released upon controller signal, with the first fin to fall pulling the remaining fins. Spring selection will depend on the size of the descent vehicle, which will determine the size of the TARRP required. For the TARRP design

investigated by the team, the value arrived at for the spring constant was 100.7 N-m/rad. This value was calculated with Equation 1 using dimensions for the rod which the fins revolve about, mass of the individual fins, the resulting moment caused by the lunar gravity at the fin's center of mass, and the angle through which the spring must act.

$$k = \frac{M}{\theta} \tag{1}$$

This system also incorporates a redundancy wherein a solenoid actuates upon receipt of the signal to deploy, providing a moment about the point of rotation to assist in the deployment of the first fin. This design is intended to be mechanically simple, and to minimize the stored volume of the final assembly while maximizing the surface area covered when fully deployed.

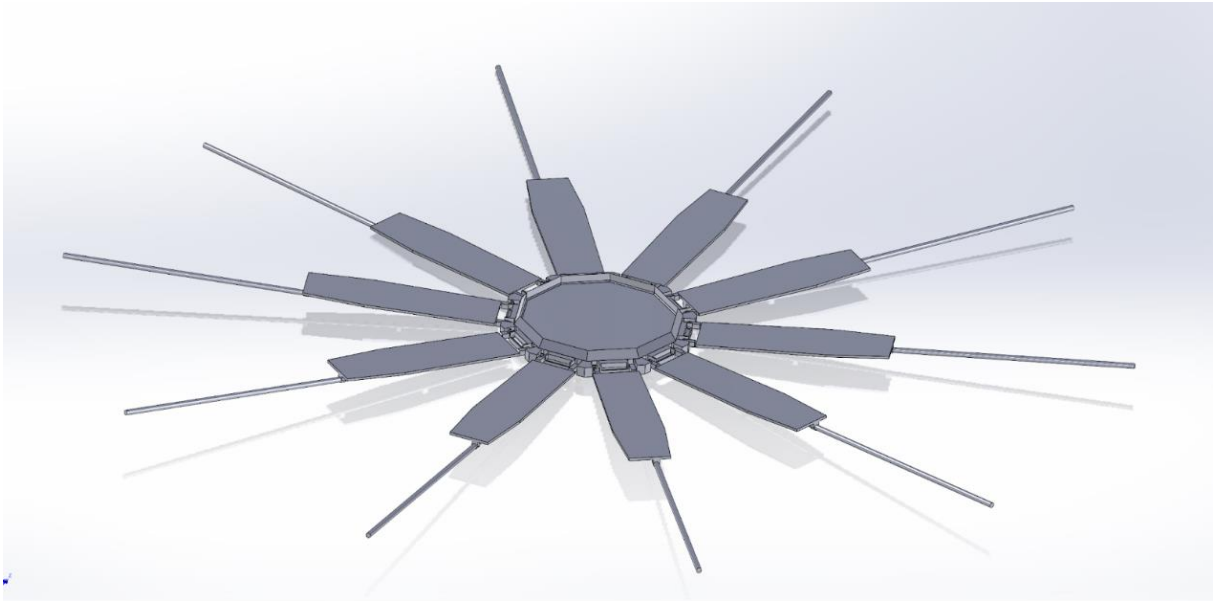

Figure 1. TARRP Baseplate and Fin Assembly. Flexible Graphite Foil not pictured.

The baseplate and fin assembly are to be composed of a carbon-matrix carbon composite material. This material was chosen for its inherent properties, such as high in-plane and relatively low cross-plane thermal conductivity [1]. The flexible material chosen for the top surface is a combination of a flexible graphite foil with a carbon felt backing. The graphite foil was chosen for its thermal properties, as well as its low permeability, preventing the plume from directly contacting the lunar regolith beneath the TARRP. The carbon felt provides an additional layer of insulation for the baseplate and fin assembly. These materials are commonly used commercially in high temperature and vacuum environments, thus consideration could be given to evaluating the Technology Readiness

Level (TRL) of the material components as TRL 3 with further testing required to elevate them to TRL 4.

The design of the TARRP is based on several assumptions:

1) Apollo-style descent vehicle that will leave the descent stage on the lunar surface.
2) Single-use design. As the descent stage is to remain atop the landing platform, there is no expectation that the platform will be reused for multiple landings.
3) Vertical, or near-vertical landing trajectory [2]. It is assumed that suitable landing zones will be identified prior to the descent vehicle launch by the Gateway and / or the orbiting CubeSats. The descent vehicle will have a well-defined landing zone prior to launch.

The preliminary TARRP design has a dry mass of 309.82 kg. This value was estimated using SolidWorks to calculate the volume of the design and summing the product of the overall volume with the volume fractions of the materials and their respective densities. Equation 2 shows the formula used for this calculation:

$$m = \sum_{i=1}^{n} V(vf)_i(\rho)_i \tag{2}$$

Where m is the mass, V is the overall volume, vf is the volume fraction of the material, and ρ is the material density.

TARRP Delivery System

The TARRP team envisions a two-stage delivery mechanism that involves a housing containing the TARRP. This housing would attach to the exterior of the descent vehicle and automatically detach at a set elevation above the surface. This point is to be determined during the mission planning process. The module will incorporate guidance, navigation, and control (GNC), as well as independent propulsion systems, radar altimeters, and lidar scanning arrays. These systems will allow it to arrest its forward momentum and orient itself over the desired landing zone while making small adjustments as altitude decreases and resolution improves. After these adjustments have been made, the TARRP will be released at a set elevation and descend to the surface. The primary stage's attitude thrusters would then fire to prevent it from landing atop the TARRP, and could then be scuttled or recovered, depending on the ultimate material condition. Upon reaching the surface, the TARRP will deploy and the HLS or CLPS will land.

The current TARRP design benefits from its relative simplicity, however, given the proposed delivery mechanism, it suffers from a large packed volume. Further design iteration would be required to reduce this packed volume to a manageable size to

accommodate final delivery to the surface. This delivery mechanism also requires that a suitable landing zone be chosen prior to launch, as the maneuverability of the TARRP module will be limited.

A sufficiently sloped lunar surface would also present a significant issue. The TARRP design could be modified with feet that would deploy to adjust its orientation. The ultimate angle would be determined by an onboard array of accelerometers and gyroscopes, with readings taken after landing, and would generate a signal for the feet to deploy. This system would only be capable of making small adjustments and would therefore be dependent on the identification of a suitable landing zone by the Lunar Gateway, HLS, and TARRP deployment module.

Deliverables

1. TARRP Testing

To determine the efficacy of the proposed solution a test environment was developed wherein a model rocket thruster was to be fired, upon both regolith and a TARRP model resting atop regolith, under vacuum conditions. The resulting deformation and erosion of the surface would then be measured using an Intel D435i depth camera, and the two cases compared to determine the overall effectiveness of the solution. Custom software was developed for the depth camera using the OpenCV framework where depth readings could be simultaneously taken from five independent points in the image, one in the center and four from the surrounding area. Figure 2. shows an early test of this program performed on a water bottle.

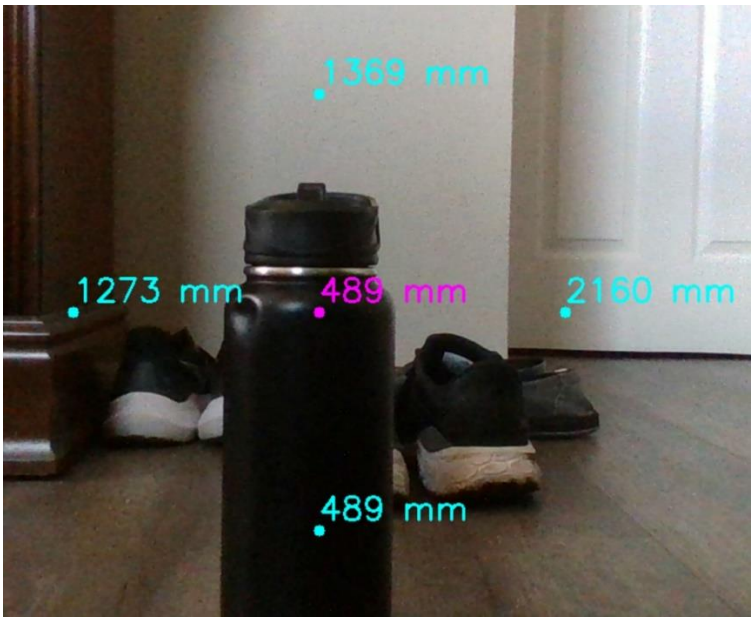

Figure 2. Depth Camera Watter Bottle Test.

Following the construction of the test environment, four validation tests were scheduled to ensure that the environment would be sufficient for testing. During the third test the environment failed, necessitating the remanufacture of a critical component. Supplemental testing was performed while the test chamber was being rebuilt.

This supplemental testing consisted of firing compressed air into the regolith surface, both with and without the TARRP model, and measuring the depth of the ultimate impingement. These tests were conducted in atmosphere. The compressed air was maintained at 100 psi and fired for 5 seconds at a height of 120 mm through a standard ¼ inch nozzle. This test was repeated six times; three tests with the TARRP, and three tests without. Table 1 shows the results of this testing, and Figures 3-8 show the readings taken from the depth camera.

Table 1. Supplemental Testing Results.

** Constant Fire Height of 120 mm was maintained w/ Fire Time of 5 seconds**			
Average Central Impingement	**Average Outer Deformation**	**Regolith Depth**	**Test**
No Mitigation			
17.5 mm	N/A	27 mm	1
17.25 mm	N/A	27 mm	2
19.75 mm	N/A	26 mm	3
TARRP Covered Surface			
0 mm	6.25 mm	25 mm	4
0 mm	10.5 mm	27 mm	5
0 mm	15.75 mm	25 mm	6

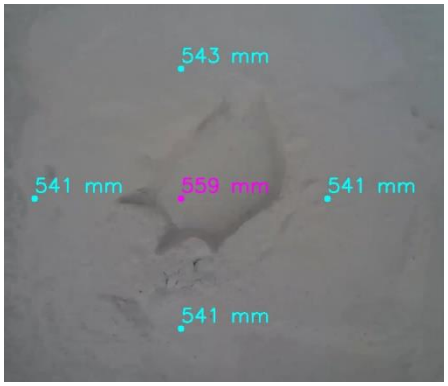

Figure 3. Test 1 Results

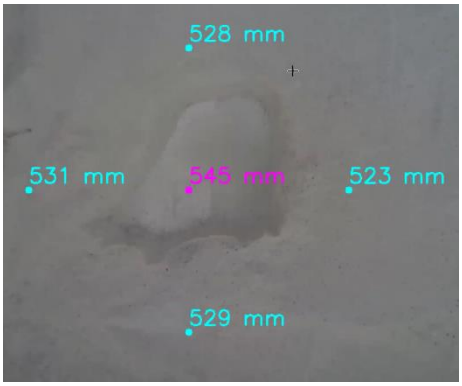

Figure 4. Test 2 Results

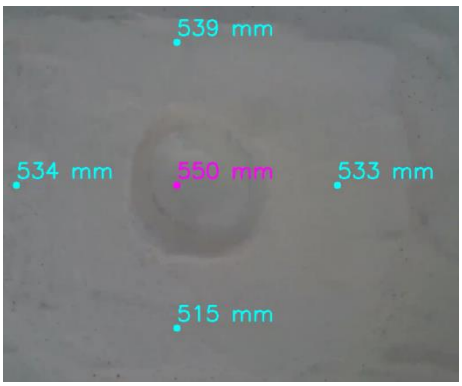

Figure 5. Test 3 Results

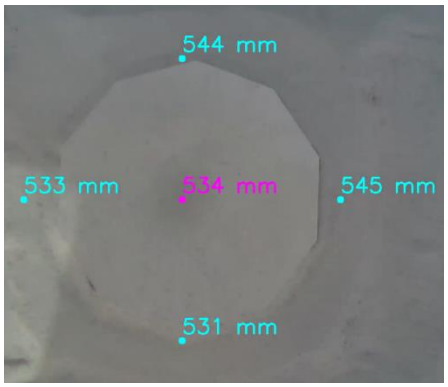

Figure 6. Test 4 Results

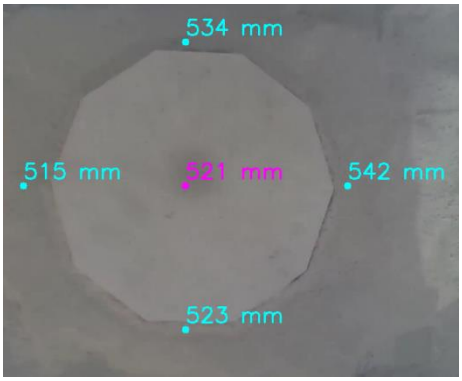

Figure 7. Test 5 Results

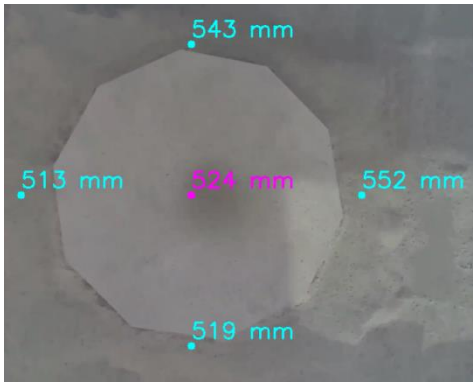

Figure 8. Test 6 Results

Results indicate zero impingement at the center of the TARRP and an average across three tests of 10.8 mm of impingement at the immediate edges. Tests without the TARRP averaged 18.2 mm impingement at the center of the jet. These results indicate that the TARRP can effectively stabilize the regolith in the immediate vicinity of the landing zone.

The test environment remanufacturing has been completed. However, due to time constraints, as of this writing final testing was unable to be conducted. Recommendations for further testing include the utilization of a larger test environment to better simulate the conditions on the lunar surface, and implementation of additional depth cameras to better capture results. Further testing will also be required to ensure that the materials chosen can withstand the stresses inherent to the application.

2. Simulation

The simulation component is intended to supplement the physical test results and to capture PSI data that would be difficult to otherwise gather (such as vorticity of the flow, and velocity and acceleration of the regolith particles). The simulation component was inspired by similar research conducted by NASA and other institutions [3 – 12].

Twenty total simulations were conducted in ANSYS Fluent Software. Four of these simulations were conducted without the TARRP in the chamber, and sixteen were conducted with the TARRP. All of these simulations were treated as 2-Dimensional, Euler-Euler multiphase problems. Symmetry was used to minimize calculation time. Regolith depth above the impermeable surface varied between 15 – 30 mm in 5 mm increments. Rocket Nozzle height above the impermeable surface varied between 50 – 200 mm in 50 mm increments.

The simulations treated the exhaust – regolith interaction as the interaction between two fluids. The regolith was considered spherical grains with a mean particle diameter of 60 μm and a density of 1.27 g/cm^3. These properties were chosen to match those of the simulant regolith used in the physical testing. The exact formulation for the rocket fuel used in physical testing (Aerotech G80-13T Model Rockets) is protected by a trade secret designation, and thus a stoichiometric analysis was impossible. Atmospheric air properties were used in the simulation in place of the rocket exhaust. Exhaust velocity was determined using Equation 3:

$$V = \frac{F}{\frac{dm}{dt}} \tag{3}$$

Where *F* is the average thrust of the rocket (77.6 N), and $\frac{dm}{dt}$ is the rate of change of the fuel mass (~36.8 g/s). Assuming the fuel is completely combusted at a uniform rate, this equation yields a velocity of 2110.7 m/s.

The region under investigation was bounded on the top and right sides by absolute vacuum, and the left side was taken as symmetry. In simulations with the TARRP, the TARRP was modeled as a stationary wall with dimensions of 133.35 mm x 3.18 mm, corresponding to those of the average radius and thickness of the scaled TARRP used in testing. A 2.5 mm mesh was used, and the simulation was initialized and run using the above conditions for 1000 time steps, with each time step representing 2.5 milliseconds. Figure 9 shows the 200 x 200 mm geometry patched with the regolith at a depth of 15 mm.

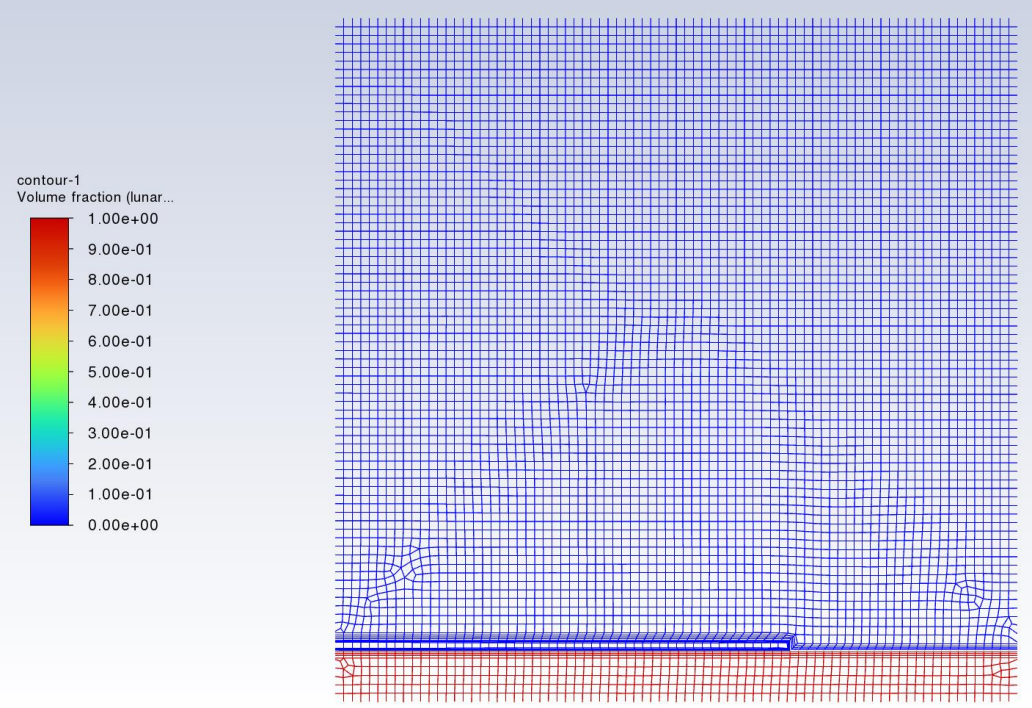

Figure 9. 200 x 200mm Region Patched with Lunar Regolith at 15mm Depth.

The TARRP simulation results universally showed an excavation of regolith from underneath the TARRP due to the no-slip boundary condition that exists at the TARRP surface. The flowlines traced the outer edge of the TARRP, and the resulting shear forces on the surface of the regolith removed the material over time. As the simulations continued to run, a gap eventually formed between the regolith surface and the bottom surface of the TARRP. Figure 10 shows the final frame of the 200 x 200mm, 20mm depth simulation with the gap visible. All simulations without the TARRP in place were completely evacuated of regolith within 100 milliseconds of simulation time.

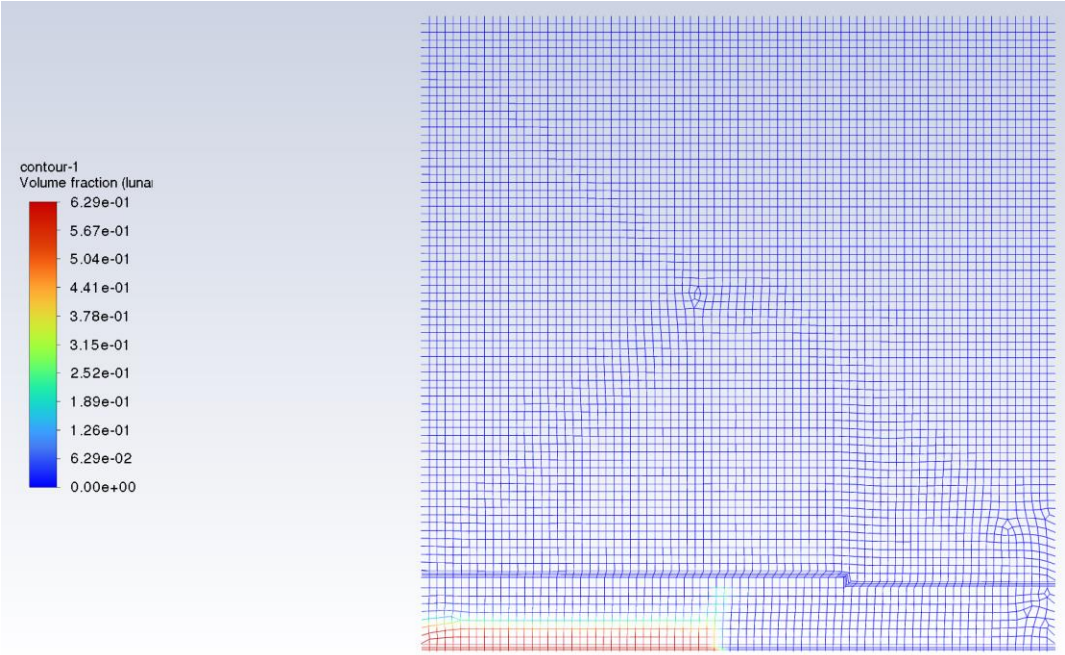

Figure 10. Final frame of 200 x 200mm Simulation with 20mm depth Regolith. Gap is visible beneath the TARRP.

Recent research performed by Dr. Philip T. Metzger of the Florida Space Institute [13-14] however, suggests that saltation plays little to no role in the erosion of regolith during lunar landings. This gives reason to believe that, by modifying the geometry of the TARRP such that there exists a slight angle at the extremities, much of this erosion could be prevented. This can be easily achieved with the current design by adjusting the terminal angle at which the fins come to rest.

3. Project Path-to-Flight Timeline and Budget Estimate

Preliminary cost estimates show a total project cost of $593.5 M. This includes costs for production, test system hardware, avionics, flight software development, system integration / assembly over a project lifetime of 5 years, and a 20% reserve. These costs are calculated using 2025 dollars and assume a total production of 20 units and 12 flights. Excess units account for potential difficulty in securing material supply, production defects, or damage incurred due to shipping, handling and packaging. Cost estimations were prepared using NASA Project Cost Estimation Capability (PCEC). Work Breakdown Structure for the TARRP is shown in Figure 11.

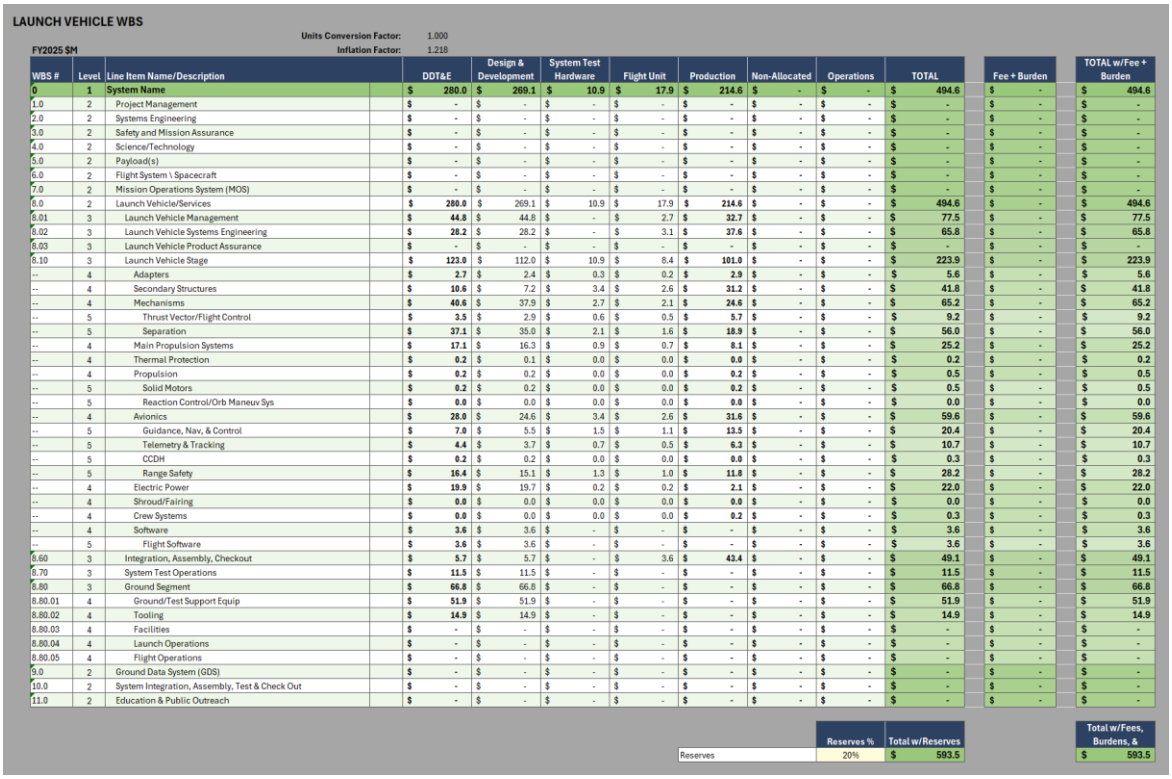

LAUNCH VEHICLE WBS

Units Conversion Factor: 1.000
FY2025 $M Inflation Factor: 1.218

WBS #	Level	Line Item Name/Description	DDT&E	Design & Development	System Test Hardware	Flight Unit	Production	Non-Allocated	Operations	TOTAL	Fee + Burden	TOTAL w/Fee + Burden
0	1	System Name	$ 280.0	$ 269.1	$ 10.9	$ 17.9	$ 214.6	$ -	$ -	$ 494.6	$ -	$ 494.6
1.0	2	Project Management	$ -	$ -	$ -	$ -	$ -	$ -	$ -	$ -	$ -	$ -
2.0	2	Systems Engineering	$ -	$ -	$ -	$ -	$ -	$ -	$ -	$ -	$ -	$ -
3.0	2	Safety and Mission Assurance	$ -	$ -	$ -	$ -	$ -	$ -	$ -	$ -	$ -	$ -
4.0	2	Science/Technology	$ -	$ -	$ -	$ -	$ -	$ -	$ -	$ -	$ -	$ -
5.0	2	Payload(s)	$ -	$ -	$ -	$ -	$ -	$ -	$ -	$ -	$ -	$ -
6.0	2	Flight System \ Spacecraft	$ -	$ -	$ -	$ -	$ -	$ -	$ -	$ -	$ -	$ -
7.0	2	Mission Operations System (MOS)	$ -	$ -	$ -	$ -	$ -	$ -	$ -	$ -	$ -	$ -
8.0	2	Launch Vehicle/Services	$ 280.0	$ 269.1	$ 10.9	$ 17.9	$ 214.6	$ -	$ -	$ 494.6	$ -	$ 494.6
8.01	3	Launch Vehicle Management	$ 44.8	$ 44.8	$ -	$ 2.7	$ 32.7	$ -	$ -	$ 77.5	$ -	$ 77.5
8.02	3	Launch Vehicle Systems Engineering	$ 28.2	$ 28.2	$ -	$ 3.1	$ 37.6	$ -	$ -	$ 65.8	$ -	$ 65.8
8.03	3	Launch Vehicle Product Assurance	$ -	$ -	$ -	$ -	$ -	$ -	$ -	$ -	$ -	$ -
8.10	3	Launch Vehicle Stage	$ 123.0	$ 112.0	$ 10.9	$ 8.4	$ 101.0	$ -	$ -	$ 223.9	$ -	$ 223.9
--	4	Adapters	$ 2.7	$ 2.4	$ 0.3	$ 0.2	$ 2.9	$ -	$ -	$ 5.6	$ -	$ 5.6
--	4	Secondary Structures	$ 10.6	$ 7.2	$ 3.4	$ 2.6	$ 31.2	$ -	$ -	$ 41.8	$ -	$ 41.8
--	4	Mechanisms	$ 40.6	$ 37.9	$ 2.7	$ 2.1	$ 24.6	$ -	$ -	$ 65.2	$ -	$ 65.2
--	5	Thrust Vector/Flight Control	$ 3.5	$ 2.9	$ 0.6	$ 0.5	$ 5.7	$ -	$ -	$ 9.2	$ -	$ 9.2
--	5	Separation	$ 37.1	$ 35.0	$ 2.1	$ 1.6	$ 18.9	$ -	$ -	$ 56.0	$ -	$ 56.0
--	4	Main Propulsion Systems	$ 17.1	$ 16.3	$ 0.9	$ 0.7	$ 8.1	$ -	$ -	$ 25.2	$ -	$ 25.2
--	4	Thermal Protection	$ 0.2	$ 0.1	$ 0.0	$ 0.0	$ 0.0	$ -	$ -	$ 0.2	$ -	$ 0.2
--	4	Propulsion	$ 0.2	$ 0.2	$ 0.0	$ 0.0	$ 0.2	$ -	$ -	$ 0.5	$ -	$ 0.5
--	5	Solid Motors	$ 0.2	$ 0.2	$ 0.0	$ 0.0	$ 0.2	$ -	$ -	$ 0.5	$ -	$ 0.5
--	5	Reaction Control/Orb Maneuv Sys	$ 0.0	$ 0.0	$ 0.0	$ 0.0	$ 0.0	$ -	$ -	$ 0.0	$ -	$ 0.0
--	4	Avionics	$ 28.0	$ 24.6	$ 3.4	$ 2.6	$ 31.6	$ -	$ -	$ 59.6	$ -	$ 59.6
--	5	Guidance, Nav, & Control	$ 7.0	$ 5.5	$ 1.5	$ 1.1	$ 13.5	$ -	$ -	$ 20.4	$ -	$ 20.4
--	5	Telemetry & Tracking	$ 4.4	$ 3.7	$ 0.7	$ 0.5	$ 6.3	$ -	$ -	$ 10.7	$ -	$ 10.7
--	5	CCDH	$ 0.2	$ 0.2	$ 0.0	$ 0.0	$ 0.0	$ -	$ -	$ 0.3	$ -	$ 0.3
--	5	Range Safety	$ 16.4	$ 15.1	$ 1.3	$ 1.0	$ 11.8	$ -	$ -	$ 28.2	$ -	$ 28.2
--	4	Electric Power	$ 19.9	$ 19.7	$ 0.2	$ 0.2	$ 2.1	$ -	$ -	$ 22.0	$ -	$ 22.0
--	4	Shroud/Fairing	$ 0.0	$ 0.0	$ 0.0	$ 0.0	$ 0.0	$ -	$ -	$ 0.0	$ -	$ 0.0
--	4	Crew Systems	$ 0.0	$ 0.0	$ 0.0	$ 0.0	$ 0.2	$ -	$ -	$ 0.3	$ -	$ 0.3
--	4	Software	$ 3.6	$ 3.6	$ -	$ -	$ -	$ -	$ -	$ 3.6	$ -	$ 3.6
--	5	Flight Software	$ 3.6	$ 3.6	$ -	$ -	$ -	$ -	$ -	$ 3.6	$ -	$ 3.6
8.60	3	Integration, Assembly, Checkout	$ 5.7	$ 5.7	$ -	$ 3.6	$ 43.4	$ -	$ -	$ 49.1	$ -	$ 49.1
8.70	3	System Test Operations	$ 11.5	$ 11.5	$ -	$ -	$ -	$ -	$ -	$ 11.5	$ -	$ 11.5
8.80	3	Ground Segment	$ 66.8	$ 66.8	$ -	$ -	$ -	$ -	$ -	$ 66.8	$ -	$ 66.8
8.80.01	4	Ground/Test Support Equip	$ 51.9	$ 51.9	$ -	$ -	$ -	$ -	$ -	$ 51.9	$ -	$ 51.9
8.80.02	4	Tooling	$ 14.9	$ 14.9	$ -	$ -	$ -	$ -	$ -	$ 14.9	$ -	$ 14.9
8.80.03	4	Facilities	$ -	$ -	$ -	$ -	$ -	$ -	$ -	$ -	$ -	$ -
8.80.04	4	Launch Operations	$ -	$ -	$ -	$ -	$ -	$ -	$ -	$ -	$ -	$ -
8.80.05	4	Flight Operations	$ -	$ -	$ -	$ -	$ -	$ -	$ -	$ -	$ -	$ -
9.0	2	Ground Data System (GDS)	$ -	$ -	$ -	$ -	$ -	$ -	$ -	$ -	$ -	$ -
10.0	2	System Integration, Assembly, Test & Check Out	$ -	$ -	$ -	$ -	$ -	$ -	$ -	$ -	$ -	$ -
11.0	2	Education & Public Outreach	$ -	$ -	$ -	$ -	$ -	$ -	$ -	$ -	$ -	$ -

	Reserves %	Total w/Reserves	Total w/Fees, Burdens, &
Reserves	20%	$ 593.5	$ 593.5

Figure 11. TARRP Work Breakdown Structure.

This document was prepared using a modified template for a launch vehicle, and it is unclear whether some of these costs overlap with those already accounted for in the overall Artemis budget. Due to the lack of publicly available documentation on how the Cost Estimating Relationships (CERs) are calculated, there exists the potential that the total cost of the TARRP project would be significantly lower than those shown in the above table.

Path-to-Flight estimates (Figure 12) were prepared for a two-year timeline to final prototype. This is an intentionally aggressive timetable which reflects the TARRP team's understanding that the primary use case for the design begins with Artemis 3. Sixteen weeks are allocated to material validation to ensure that the TARRP itself is capable of withstanding the thermal stresses and shear forces it will be subjected to by the descent vehicle's engines. Initial design optimization will occur over the first 20 weeks, concurrently with the material validation, to ensure a better optimized initial design. Following initial prototype manufacture and testing, the remaining time is allocated for redesign, manufacturing, testing and implementation. This process is intended to be iterative and to ensure that the final product is well-suited to provide PSI mitigation for the early Artemis missions.

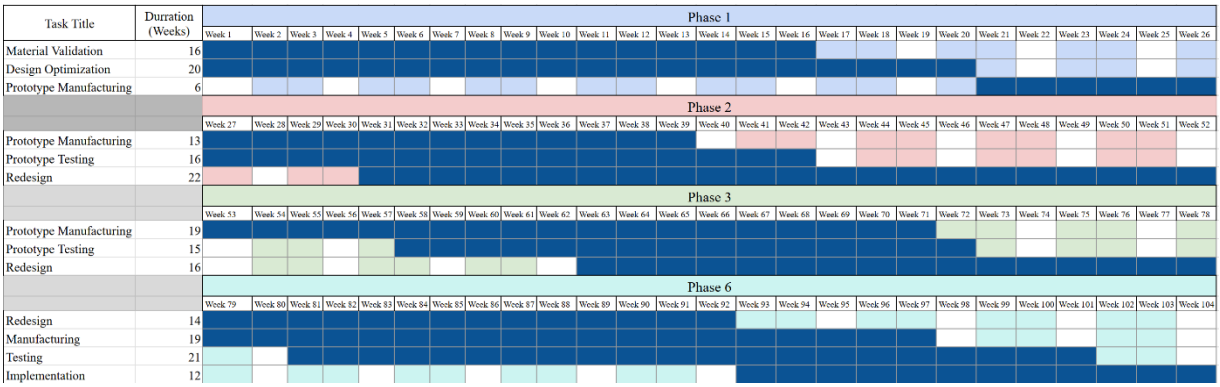

Figure 12. GANNT Chart of Project Timeline.

Appendix – Referencees and Bibliography

[1] C. Ohlhorst, W. Vaughn, and P. Ransone, “NASA Technical Memorandum 4787 Thermal Conductivity Database of Various Structural Carbon-Carbon Composite Materials,” National Aeronautics and Space Administration, Langley Research Center, 1997. Accessed: Nov. 05, 2023. [Online]. Available: https://ntrs.nasa.gov/api/citations/19970041399/downloads/19970041399.pdf

[2] M. Loucks, J. Carrico, T. Carrico, and C. Deiterich, “A Comparison of lunar landing trajectory strategies using numerical solutions,” presented at the International Lunar Conference, Accessed: Oct. 22, 2023. [Online]. Available: https://astrogatorsguild.com/wp-content/Astrogator_Training/LunarLanding.pdf

[3] Y. Mehta, R. J. Goetsch, O. V. Vasilyev, and J. D. Regele, “A particle resolved simulation approach for studying shock interactions with moving, colliding solid particles,” *Computers & Fluids*, vol. 248, no. 248, pp. 105670–105670, Nov. 2022, doi: https://doi.org/10.1016/j.compfluid.2022.105670.

[4] J. You *et al.*, “Analysis of plume–lunar surface interaction and soil erosion during the Chang’E-4 landing process,” *Acta Astronautica*, vol. 185, no. 185, pp. 337–351, Aug. 2021, doi: https://doi.org/10.1016/j.actaastro.2021.05.009.

[5] C. Q. LaMarche and J. S. Curtis, “Cratering of a particle bed by a subsonic turbulent jet: Effect of particle shape, size and density,” *Chemical Engineering Science*, vol. 138, no. 138, pp. 432–445, Dec. 2015, doi: https://doi.org/10.1016/j.ces.2015.08.030.

[6] A. M. Korzun *et al.*, “Design of a Subscale, Inert Gas Test for Plume-Surface Interactions in a Reduced Pressure Environment,” *AIAA SCITECH 2022 Forum*, Jan. 2022, doi: https://doi.org/10.2514/6.2022-1808.

[7] L. A. Florio, “Dynamic coupling of fluid and structural mechanics for simulating particle motion and interaction in high speed compressible gas particle laden flow,” *Journal of Fluids and Structures*, vol. 54, no. 54, pp. 171–201, Apr. 2015, doi: https://doi.org/10.1016/j.jfluidstructs.2014.10.014.

[8] G. Cai, B. Zhang, L. Liu, H. Weng, W. Wang, and B. He, “Fast vacuum plume prediction

using a convolutional neural networks-based direct simulation Monte Carlo method," *Aerospace Science and Technology*, vol. 129, no. 129, pp. 107852–107852, Oct. 2022, doi: https://doi.org/10.1016/j.ast.2022.107852.

[9] H. Zhang *et al.*, "The Investigation of Plume-Regolith Interaction and Dust Dispersal during Chang'E-5 Descent Stage," *Aerospace*, vol. 9, no. 7, pp. 358–358, Jul. 2022, doi: https://doi.org/10.3390/aerospace9070358.

[10]J. Capecelatro, "Modeling high-speed gas–particle flows relevant to spacecraft landings," *International Journal of Multiphase Flow*, vol. 150, no. 150, pp. 104008–104008, May 2022, doi: https://doi.org/10.1016/j.ijmultiphaseflow.2022.104008.

[11] J. West *et al.*, "Overview of the Predictive Simulation Capability Element of the Plume Surface Interaction Project," presented at the AIAA SciTech Forum.

[12] Y. Li, D. Ren, Z. Bo, W. Huang, Q. Ye, and Y. Cui, "Gas-particle two-way coupled method for simulating the interaction between a rocket plume and lunar dust," *Acta Astronautica*, vol. 157, pp. 123–133, Apr. 2019, doi: https://doi.org/10.1016/j.actaastro.2018.12.024.

[13] P. T. Metzger, "Erosion rate of lunar soil under a landing rocket, part 1: Identifying the rate-limiting physics," *Icarus*, vol. 417, pp. 116136–116136, Jul. 2024, doi: https://doi.org/10.1016/j.icarus.2024.116136.

[14] P. T. Metzger, "Erosion rate of lunar soil under a landing rocket, part 2: Benchmarking and predictions," *Icarus*, vol. 417, pp. 116135–116135, Jul. 2024, doi: https://doi.org/10.1016/j.icarus.2024.116135.

TCNJ Adaptable Regolith Retention Platform (TARRP)

Major Objectives & Technical Approach

- Objectives
  - To determine the efficacy of applying a single-use landing platform to mitigate the cratering, and expulsion of ejecta upon descent, landing and ascent caused by Plume-Surface Interaction (PSI)
- Technical Approach
  - Design a scaled prototype platform and perform experimental evaluations of the design in both a simulated environment and a vacuum chamber

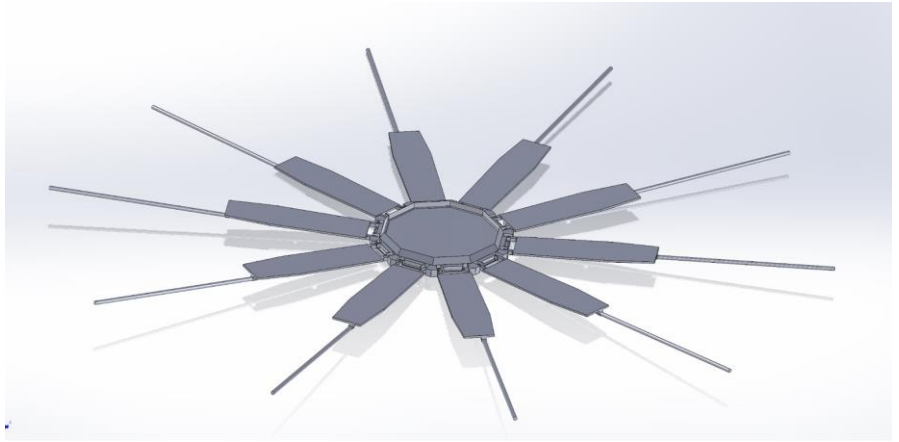

Key Design Details

- Design Details
  - Decagonal C/C composite base and fins with a lightweight graphite foil in the interstitial spaces between fins. Designed to unfold upon deployment and provide a barrier between the vehicle exhaust and the regolith
- Innovations
  - Low mass, single-use platform intended to bridge the gap between initial landings and the establishment of more permanent landing infrastructure on the lunar surface via rapid sintering of regolith or other emerging solutions

Summary of Schedule & Costs

- Schedule
  - Two-Year timeline for design iteration, prototype manufacturing and testing.
  - Expected Five-Year Mission Timeline
- Costs
  - Per prototype manufacturing costs of approx. $21,713 and total project cost of $593.5 M